

The stochastic nature of migration of disc instability protoplanets in three-dimensional hydrodynamical and MHD simulations of fragmenting discs

Noah Kubli,^{1*} Lucio Mayer,¹ Hongping Deng,² Douglas N. C. Lin^{3,4}

¹ *Department of Astrophysics, University of Zurich, Winterthurerstrasse 190, CH-8057 Zürich, Switzerland*

² *Shanghai Astronomical Observatory, Chinese academy of Science, Nandan Rd 80th, 200030 Shanghai, China*

³ *Department of Astronomy and Astrophysics, University of California, Santa Cruz, CA 95064, USA*

⁴ *Institute for Advanced Studies, Tsinghua University, Beijing 100084, China*

Accepted XXX. Received YYY; in original form ZZZ

ABSTRACT

We present a detailed analysis of the nature of migration of protoplanetary clumps formed via disc instability in self-consistent 3D hydrodynamical (HD) and magneto-hydrodynamical (MHD) simulations of self-gravitating discs. Motivated by the complex structure of protoplanetary clumps we do not introduce sink particles. We find that the orbital evolution of the clumps has a stochastic character but also exhibits recurrent properties over many orbits. Clump migration is governed by two sources of gravitational torques: a torque originating from a region about twice the Hill sphere around each clump’s orbit, and the torque resulting from clump-clump interactions. Compared to non-magnetized companion runs, the latter are more frequent in MHD simulations, which give rise to more numerous clumps starting off at smaller masses, often below a Neptune mass. Clump-clump interactions can lead to temporary strong accelerations of migration in both directions, but integrated over time provide a lesser impact than disc-driven torques. They can also lead to clump mergers but do not cause ejections; a difference to previous works which adopted sink particles. The local “Hill torque” is responsible for the fast migration, inward or outward. Estimating the characteristic timescales of conventional migration in our regime, we find that the disc-driven migration timescales are in agreement with Type III migration. However, the dominant local torque is rapidly fluctuating, which reflects the turbulent nature of the flow. The resulting stochastic migration pattern is markedly different from Type III runaway migration and appears to be a distinctive feature of orbital dynamics in a fragmenting disc.

Key words: planet–disc interactions – MHD – planets and satellites: formation

1 INTRODUCTION

Gravitational instability (GI) (Kuiper 1951) is a possible formation path of planets. For sufficiently cold gas, gravity may dominate over shear and pressure forces leading to a local collapse in the protoplanetary disc (Toomre 1964; Boss 1997; Mayer et al. 2002). Although conventional wisdom attributes a lesser role of disc instability theory relative to the core accretion (CA) theory (Safronov 1972; Pollack et al. 1996; Johansen & Lambrechts 2017) in the process of planet formation, the relative importance of the two modes of planet formation is still not clear. For very massive planets $> 4M_J$ the correlation between metallicity and giant planet occurrence observed at lower masses is no longer present, disfavoring CA as the formation path for these planets (Santos, N. C. et al. 2017). Furthermore, CA has problems in explaining the observed vast population of intermediate-mass planets (Suzuki et al. 2018; Schlecker, M. et al. 2022). Finally, the wide-orbit exoplanet population discovered by imaging surveys is becoming more numerous as time progresses and is hosted by a wide range of stellar types (Marois et al. 2008; Bohn et al. 2020;

Janson et al. 2021; Delorme et al. 2024). While this is not necessarily incompatible with CA, it is more naturally explained by GI. In both formation scenarios, planets are thought to migrate radially (Goldreich & Tremaine 1980; Vorobyov & Basu 2005; Baruteau et al. 2011) because of interactions with the disc in which they are embedded as well as due to gravitational interactions with other planets. Simple semi-analytical models of migration in GI have shown that it can significantly affect the orbital distribution of planets after birth, which, contrary to naive expectations, can result in a population of Hot Jupiters as well as of wide-orbit planets (Galvagni & Mayer 2013; Müller et al. 2018).

Global spiral structure in protoplanetary discs in their early phases, the signpost of GI, have been observed several times (Pérez et al. 2016; Meru et al. 2017; Veronesi et al. 2021; Speedie et al. 2024) confirming that at least some discs may be gravitationally unstable (Toomre 1964; Deng & Ogilvie 2022). In a few cases even an analysis of the disc kinematics has been possible, leading to results compatible with a self-gravitating disc (Veronesi et al. 2024).

Simulations of GI predict a wide range of fragment masses and radial separations from the host star, from brown dwarfs and binary stellar companions down to giant gas planets (Boss 1997; Mayer et al. 2004). Recently, the first MHD simulations of GI showed frag-

* E-mail: noah.kubli@uzh.ch

mentation at much smaller scales in the intermediate-mass regime, generating Neptune-sized as well as Super-Earth-sized clumps (Deng et al. 2021; Kubli et al. 2023). In the latter, magnetic fields stifle accretion via magnetic pressure, thus suppressing mass growth after birth, and also shield them from disruption, thus allowing them to survive shear stresses and stellar tides despite their lower masses. Magnetic fields in GI discs are amplified and sustained through the spiral density waves by means of the so-called “GI dynamo” (Deng et al. 2020).

Disc instability is favoured in the early evolutionary stage of the disc, in Class 0-1, when it should be more massive and still accreting, two factors that can concur to trigger GI and disc fragmentation (Boley 2009; Hayfield 2011). It is therefore interesting to investigate the fate of such clumps with respect to radial migration using simulations. In the pure form of GI, the planet masses are correlated with the distance to the central star. Similar to the CA model, migration and other processes, such as gas accretion (Zhu et al. 2012; Stamatellos 2015), clump-clump collisions with various outcomes (Matzke et al. 2024), pebble accretion (Humphries & Nayakshin 2018), and tidal disruption and downsizing (Nayakshin 2010) have to be taken into account in order to explain the observed planetary population (Nayakshin & Fletcher 2015).

In contrast to conventional migration theory (Goldreich & Tremaine 1979; Lin & Papaloizou 1979; Tanaka et al. 2002a), the presence of GI adds additional effects: the self-driven spiral patterns can induce torques on the (proto-)planets leading to more chaotic dynamics (Baruteau et al. 2011), and clumps can interact with one another (Cha & Nayakshin 2011; Hall et al. 2017). Therefore simulations are needed to investigate migration in such discs. Migration in gravitationally unstable discs has been investigated since more than a decade using simulations. Among the pioneering works is Baruteau et al. (2011), who found inward migration on a time-scale of 10 outer disc orbital periods using 2D simulations of individual protoplanets in a GI disc. Other 2D simulations are used in Machida et al. (2011) where they found infall of fragments on to the host star explaining intermittent stellar outflows such as FU-Ori bursts. Malik et al. (2015) investigated the gap opening criterion in both non-self-gravitating and GI discs, for both Type I and Type III migration of gas giants and brown dwarfs (Masset & Papaloizou 2003a; Masset 2008; Pepliński et al. 2008; Baruteau & Masset 2008a; Lin & Papaloizou 2012) and found that gap-opening is more difficult than previously thought because a short migration time scale compared to the orbital time can prevent the opening of a gap where the conditions would otherwise be met. In particular, in GI discs migration turned out to be often in the fast Type III regime, preventing gap formation. On the other hand, Rowther & Meru (2020) found that migration can be slowed down in GI discs once clumps enter the hot gravitationally stable inner disc. Fletcher et al. (2019) carried out the first extensive code comparison focused on migration of clumps that were formed in self-gravitating (SG) discs. The GIZMO code (Hopkins 2015) we used in this paper was part of the suit of employed codes. They found that the codes agreed qualitatively yet the migration rate differed by up to 50%. To reduce complexity, they imposed a Toomre Q parameter near unity as expected in a GI disc but without letting the disc fragment, and inserted a planet represented by a sink particle with a mass and a formation location in the range expected for GI discs.

In most studies of migration in the disc instability scenario, as those just described, only a single clump is considered, using a sink particle (which can be accreting or not) in a background disc that is marginally gravitationally unstable but not fragmenting (e.g. Baruteau et al. (2011); Michael et al. (2011); Malik et al. (2015); Stamatellos (2015)). This is in contrast with the expected configura-

tion arising in fragmenting discs, in which clumps are numerous and evolve in a disc that has fragmented, which then supports a highly gravito-turbulent flow (Durisen et al. 2007). In self-consistent simulations of fragmenting discs, the clumps also mutually interact, can merge, and also accrete gas further while migrating. In Boss (2013) and Boss (2023), using two different Eulerian hydrodynamics codes with flux-limited diffusion, they improved the realism of migration studies by simulating a disc in the fragmenting regime and inserting not one but multiple clumps, represented as sink particles, in the density maxima of spiral arms where they expect fragmentation to happen. In Boss (2023) the clumps were also allowed to merge. However, when employing sink particles, gravitational interactions and also disc-protoplanet interactions are altered as the clumps are not deformable. Rather they are rigid bodies, with their interiors being unresolved, a simplification that completely suppresses the effect of shear and tidal forces. This would indirectly affect the migration rate, as tidal downsizing of clumps (Boley et al. 2010; Nayakshin 2010) would slow migration considerably, an effect that has been shown to be statistically important in population synthesis models (Galvagni & Mayer 2013; Müller et al. 2018). By missing the effect of tides, sinks also miss an important component: the angular momentum exchange phenomenology. Further the choice of softening of the sink particles’ potentials adds more free parameters to the simulation and alters the strength of clump-clump interactions. In Boss (2013), inward and outward migration is observed, and a few protoplanets are also scattered out of the disc, potentially leading to free-floating planets.

In this work we carry out a self-consistent study of migration of protoplanetary clumps in fragmenting discs, examining for the first time migration in both hydrodynamical and MHD simulations. We intentionally do not replace the clumps with sink particles. This allows us to fully assess the effect of clump-clump interactions in migration, and to fully account for the interplay between accretion, tidal mass loss and migration.

2 METHODS

2.1 Numerical methods

We analyze the simulations described in Deng et al. (2020, 2021); Kubli et al. (2023). These are fully three-dimensional, self-gravitating simulations of a protoplanetary disc and further include the magnetic field. The simulations have a very high resolution, with a particle mass of $2 \times 10^{-6} M_{\text{jup}}$ in the MHD runs and $2.4 \times 10^{-5} M_{\text{jup}}$ in the HD run. The gravitationally bound clumps which have sizes in the range of 0.1 to 0.9 AU are resolved with $\approx 5000 - 100000$ particles, hence their internal structure is at least partially resolved.

Both the clumps (protoplanets) and the magnetic field emerge self-consistently meaning their properties (mass / orbit of the clumps, strength and alignment of the magnetic field) are not free parameters in the simulation but they emerge through integrating the physical equations. The simulation solves the MHD equations with self-gravity. The magnetic component includes Ohmic diffusivity with $\eta = c_s H / 25$ where c_s and H are the sound speed and the disc scale height at the radial position of the fluid element. The energy equation contains a cooling term with a cooling time $\tau_c = \beta \Omega^{-1}$ where Ω^{-1} is the local orbital time scale:

$$\frac{\partial \rho}{\partial t} + \nabla \cdot (\rho \mathbf{v}) = 0 \quad (1)$$

$$\frac{\partial \mathbf{v}}{\partial t} + \mathbf{v} \cdot \nabla \mathbf{v} = -\frac{1}{\rho} \nabla(P + \frac{\mathbf{B}^2}{8\pi}) + \frac{(\mathbf{B} \cdot \nabla) \mathbf{B}}{4\pi\rho} - \nabla\Phi \quad (2)$$

$$\frac{\partial \mathbf{B}}{\partial t} = \nabla \times (\mathbf{v} \times \mathbf{B}) + \eta \nabla^2 \mathbf{B} \quad (3)$$

$$\frac{\partial U}{\partial t} + \nabla(U\mathbf{v}) = -P\nabla\mathbf{v} - \frac{U}{\tau_c}. \quad (4)$$

To solve the equations, we use GIZMO (Hopkins 2015; Hopkins 2016; Hopkins & Raives 2016). The simulations assume an ideal monatomic gas with adiabatic exponent $\gamma = 5/3$ and equation of state $P = (\gamma - 1)U$. The cooling constant β is varied during the earlier phases of the simulation (see section 2.2). The gravitational softening is adaptive with a lower limit of 0.05 AU (Price & Monaghan 2007). The central star is represented as a single sink particle starting with $1M_{\text{sun}}$. Particles falling into the sink radius, which is chosen to be 5 AU are removed and their mass and momentum is added to the star.

2.2 Initial setup and fragmenting stage

The initialization stage is described in Deng et al. (2020). The simulations start with an axisymmetric disc with a radial extension of 5–25 AU, a surface density profile of $\Sigma \propto r^{-1}$ and a temperature profile of $T \propto r^{-1/2}$. The local scale height of the disc was chosen such that it is in pressure-gravity equilibrium. The initial disc mass is $\approx 0.1M_{\text{sun}}$, representing an earlier stage of a protoplanetary disc’s evolution where gravitational instability is present. A toroidal seed magnetic field was further introduced which grows through the GI dynamo into an equilibrium configuration over some orbits. To avoid numerical fragmentation, a weak cooling rate of $\beta = 8$ was used until the establishment of a spiral structure through out the disc (Meru & Bate 2011; Deng et al. 2017). The cooling was then increased to the desired $\beta = 2\pi$ until the disc saturated to a quasi-equilibrium state with vigorous MHD turbulence powered by the spiral density waves (Riols & Latter 2019; Deng et al. 2020). To trigger fragmentation we switched to a faster cooling of $\beta = 3$ (Gammie 2001; Deng et al. 2017). This led to the formation of clumps over a range of different sizes. This is described in Kubli et al. (2023) and Deng et al. (2021). Most importantly, the fragments in the MHD case are of significantly lower mass than in the HD case, with many initial masses below the mass of Neptune. To follow the clump’s evolution and their interactions the system was then evolved by switching back to $\beta = 2\pi$ to avoid runaway fragmentation. This corresponds to the time $t = 0$ in the surface density plots of fig. 1. As shown in Kubli et al. (2023), the clumps have a complex internal structure, exhibiting flattened non-axisymmetric shapes and possessing significant angular momentum. Additionally, clumps in MHD and HD simulations also show structural differences. This suggests that treating them as sink particles would not capture their mutual dynamical interaction correctly, and also affect the exchange of angular momentum with the disc. Since we want to understand the physics of migration at some depth, we prefer to give up running for long timescales, an inevitable issue as clumps contract and the integration time-step becomes increasingly small, and rather make sure to fully capture the dynamical interaction with the disc and between clumps for as many orbits as we can follow the system.

Due to the expected self-shielding in the interiors of the clumps it is physically reasonable to deactivate cooling in the cores. In a subset of our simulations this is done by setting a density threshold

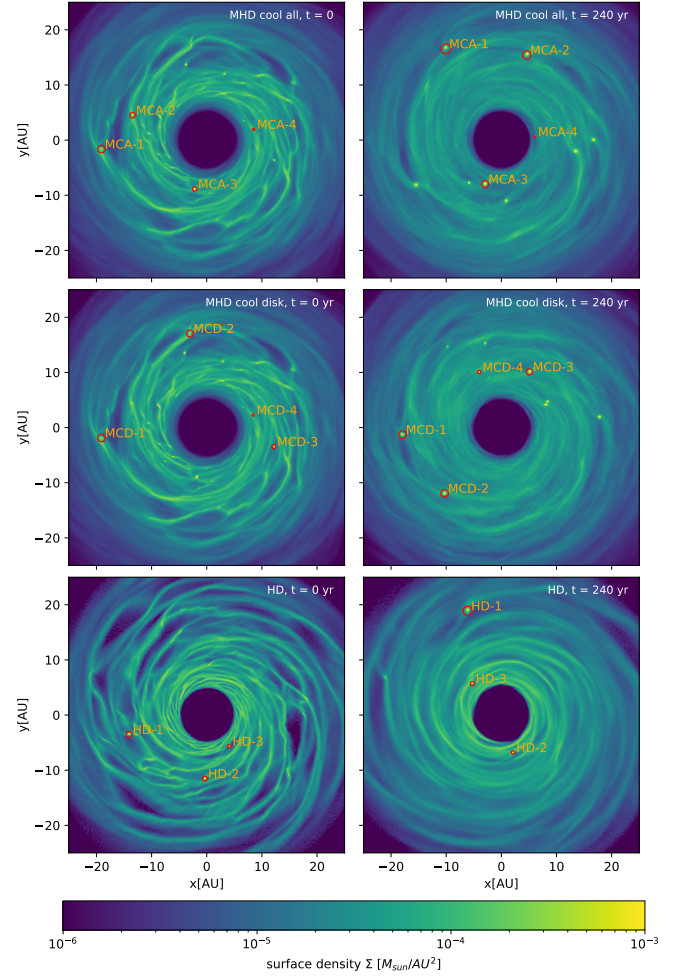


Figure 1. Surface density plots of the three runs at the beginning (left) and at a later stage $t = 240$ yr. Top: *MHD cool all*, including the magnetic field and applying beta cooling on the whole system. Middle: *MHD cool disc*, including the magnetic field and applying beta cooling *only* to the disc, not the interior of the clumps. Bottom: *HD*, neglecting the magnetic field and applying beta cooling to the whole system.

of 10^{-9} g/cm^3 (see Deng et al. (2021)) above which beta-cooling is not applied. The corresponding run is dubbed *MHD cool disc* (*MCD*). Two companion runs are also used for the analysis. In *MHD cool all* (*MCA*) radiative cooling remains active also in the clump interior. This leads to a more pronounced collapse and a higher accretion rate on to the clump making them more massive over time as shown in fig. 2. In *HD* the magnetic field is neglected hence this run takes into account only the hydrodynamics and the disc’s self-gravity. The surface density plots in fig. 1 show a visible difference between the magnetized and the unmagnetized runs: in the magnetized case the global spiral modes are less pronounced but there is more small scale structure, including higher frequency spiral modes (Deng et al. 2020).

2.3 Torque decomposition

In this section we describe how we compute the torque that is exerted on the clumps and how we isolate its components. For each clump, we start by computing the gravitational acceleration (specific force) a_g on the clump’s centre of mass. Here we take into account all the

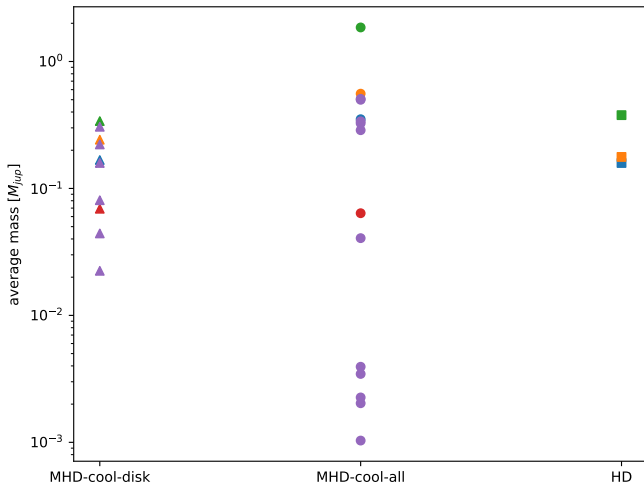


Figure 2. Average masses of the clumps over their lifetime in different runs. In the magnetized runs, there are more fragments than in the purely hydrodynamical (HD) runs. The magnetic field also allows for fragmentation at lower masses. In *MHD cool all*, where the interiors of the clumps are also cooled, some clumps grow to much higher masses during the course of the simulation.

disc’s particles but exclude the other particles of which the clump itself consists. The specific gravitational torque is then simply

$$\boldsymbol{\mu} = \boldsymbol{r} \times \boldsymbol{a}_g, \quad (5)$$

with \boldsymbol{r} being the clump’s position measured from the disc centre. Assuming a circular orbit, the specific torque can directly be related to a change in radius:

$$(\boldsymbol{r} \times \boldsymbol{a}_g)_z = \frac{\dot{r}}{2\sqrt{r}}. \quad (6)$$

At each snapshot, the total torque is evaluated and the radius integrated. Theoretically this should give us the exact evolution of the radial positions since pressure or magnetic forces are not expected to be important on the clump’s orbital evolution. However since the analysis is done on the snapshots that are available in discrete time intervals of ≈ 1.6 yr, some information is missing and the prediction will not be exact. Further the clump’s orbits are not purely circular but may have some eccentricity. In practice the approximation works reasonably well for our purposes (see section 3.1).

In the conventional linear migration theory giving rise to Type I migration the contribution to the torque outside the co-rotation region comes from the sum of the resonant torques at the Inner and Outer Lindblad Resonances (ILR and OLR) located, respectively, further in and further out than the clump’s orbit (Lin & Papaloizou 1986a). An additional contribution comes from material that co-rotates with the clump (Tanaka et al. 2002b). Analogously, in our analysis we dissect the torque on each clump into different components and attribute the corresponding migration effects to each of them. We define the following components:

- The **clump-clump torque** is the torque arising from interactions between two or more clumps.
- The **disc torque** is the torque arising from the rest of the material (excluding other clumps). We divide it further into different parts; the following components are all a part of the disc torque.
- The **outer disc torque** (part of the disc torque) is the torque contribution from all matter on orbits further *outside* than a Hill radius as measured from the respective clump, while excluding clump-clump interactions.

- Vice-versa, the **inner disc torque** (part of the disc torque) is the torque contribution from all matter on orbits further *inside* than a Hill radius as measured from the respective clump, also excluding clump-clump interactions.

- Then we measure the remaining **torque from within 1 Hill radius** (part of the disc torque) around the clump’s orbit. Also here, clump-clump interactions are excluded. We treat this part of the torque separately (not in the inner / outer torque) because the material on orbits close to the protoplanets is where we expect to be most of the contribution. Indeed, massive planets in massive discs can, in principle, enter the Type III or runaway regimes, in which the dominant contribution of the torques comes from the material in the co-rotating region or near to it (see e.g. Papaloizou et al. (2007)).

- Although the above decomposition is complete (summing all contributions equals the total torque) we also show the **torque from within 2 Hill radii** (part of the disc torque) around the clump’s orbit (excluding clump-clump interactions). We do this to investigate what region around the clump’s orbit is mostly responsible for the disc torque.

We want to stress here that our simulations have a highly non-linear flow as the disc is self-gravitating and turbulent, due to gravito-turbulence (magnetized and HD runs) and MHD turbulence (magnetized runs). Both, gravitational stresses and Maxwell stresses are high in the MHD simulations (Deng et al. 2020). Therefore, our flow conditions are at odds with the assumptions made in linear theory. However, the eventual contribution of resonant torques at ILRs and OLRs, if relevant, is automatically included in, respectively, the inner and outer disc torque, which should be interpreted as a radially integrated torque. It will still be instructive, a posteriori, to compare our results with the expectation of linear torque theory, in particular to compare with Type I migration torques and their timescales, and to check if there is evidence of an important contribution at the expected location of the resonances.

3 RESULTS

3.1 Radial migration and torque-based predictions

We will start by assessing the robustness of our torque measurement, and then consider separately the different torque components defined in the previous section to uncover the in-depth nature of migration for disc instability protoplanets. For each different run we chose at most four exemplary clumps which we show individually in the plots except when we use the full sample for generating statistical diagnostics, and use the same colours for them. The solid lines in fig. 3 show the observed radial positions of the clumps in the simulation. One can see that there is considerable change of the radial positions over time. For example, over ~ 5 orbits, clump MCD-1 changes its radial position from 20 AU to 16 AU and clump MCA-4 changes its position rapidly from ~ 10 AU to 7 AU. Some clumps have a somewhat high eccentricity (e.g. MCA-3 and MCA-4). Besides inward-directed migration there is also outward-directed migration (clump MCD-4 of the ones shown). The motions seem to have a large stochastic component.

First we verify that our method to estimate the torque at the (radial) location of the clump, described in section 2.3, is quantitatively consistent with the time evolution of the semi-major axis of clumps observed in the simulation. We show the result in fig. 3 for four exemplary plots in both MHD runs. The dashed lines, representing the predicted positions of the clumps, closely follow the solid lines, representing the actual positions of the clumps. We did not take into

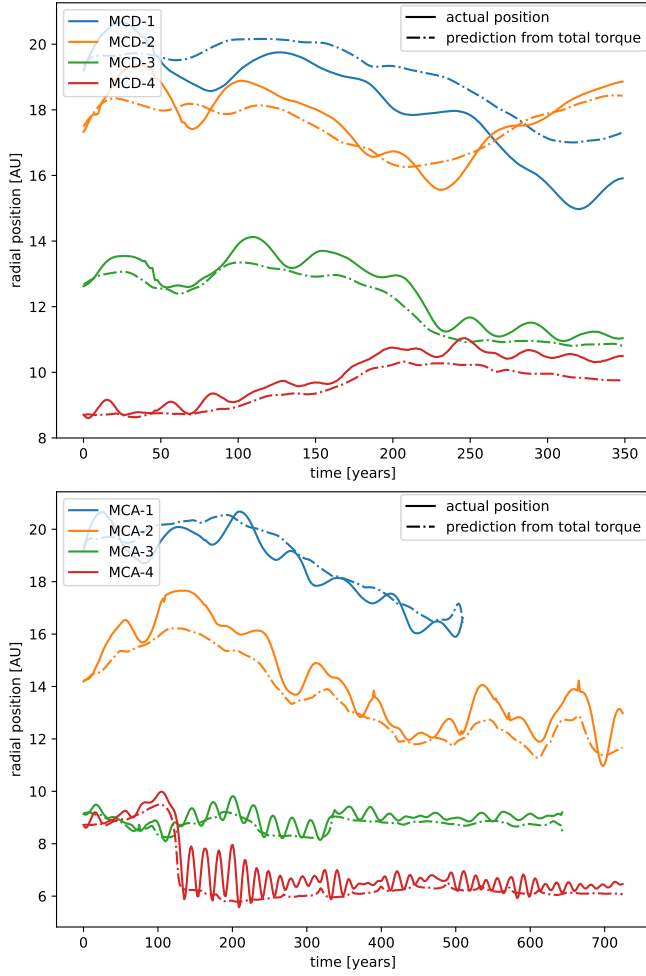


Figure 3. Radial positions of four exemplary clumps (solid lines) and their projected positions using the torque computed from the simulation snapshots. The evolution of the radial position is well described using this method.

account the eccentricity of the clumps when integrating the torque, but the prediction represents reasonably well an orbital average of the clumps. This already shows that the torque is mediated through the self-gravity of the gas and we can neglect any direct effects of the pressure forces and the magnetic field on the migration of the clumps. Of course these forces are important when shaping the global structure of the disc and therefore influence the final torque arising from the self-gravity.

3.2 The components of the torque

The effects of the different torque components are summarized in fig. 4. In both plots we show the radially migrated distance of each clump. In the later plots of individual clumps they are marked with the same colours. All the other clumps found in the simulation, not shown individually in other plots, are shown in transparent purple. The effects attributed to the different torque components are shown in each column.

The first column shows the total migrated distance over the simulation time for each clump. In all runs we have in- and outward migration. The next column represents migration due to clump-clump interactions. This is calculated by integrating the clump-clump torque (see section 2.3). The importance of this component is different be-

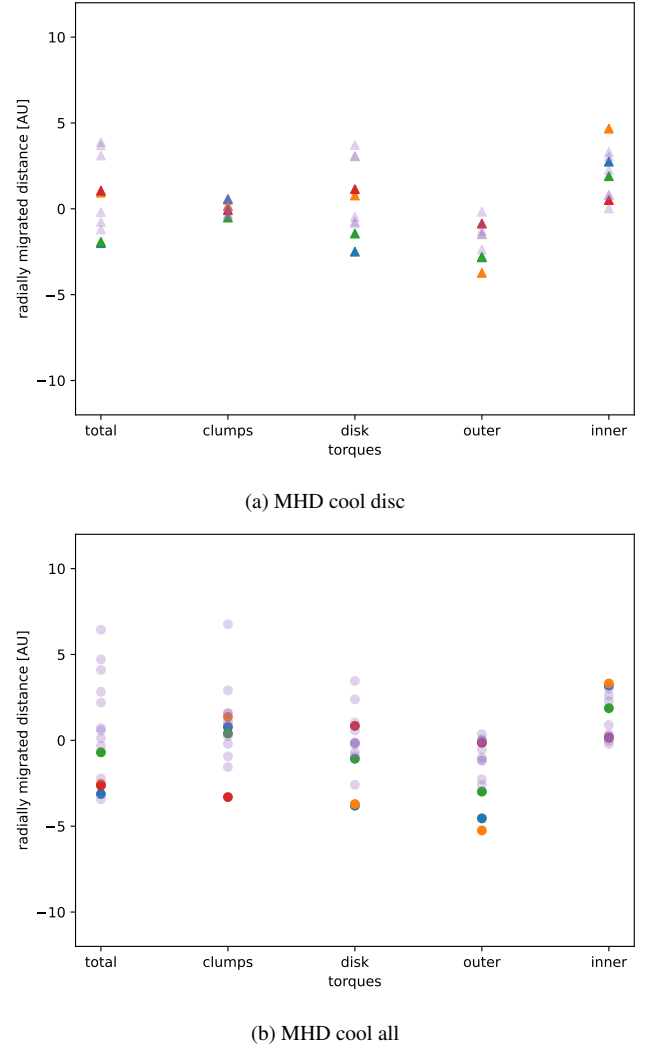


Figure 4. Change in radial position arising from different components of the torque. The effect of clump-clump interactions is much higher in the *MHD cool all* case, consistent with the higher masses. It can be seen that the outer torque leads to inward migration while the inner torque leads to outward migration in both cases.

tween the two magnetized runs *MHD cool disc* and *MHD cool all*. In the run *MHD cool disc* clump-clump interactions only account for a fraction of the total migration whereas in *MHD cool all* clump-clump interactions play a significant role. This is probably due to the higher masses arising in *MHD cool all* (see section 2.2). We note here that the run *MHD cool disc* is probably more realistic because cooling was turned off in the clump cores, which accounts for the self-shielding. In such a case we expect migration to be dominated mostly by the interactions with the gas disc whereas clump-clump interactions add stochastic perturbations.

The other three columns to the right display the effect of the disc. The outer and inner torque result from the previously defined decomposition of the disc torque (see section 2.3). The picture here is similar in both the magnetized and the unmagnetized runs. It can be noted that the outer disc torque is mostly responsible for inward migration, thus it imparts a negative torque component, whereas the inner torque leads mostly to outward migration (see section 3.4). This is consistent with expectations from Type I migration theory where the inner Lindblad resonance causes a positive torque and the outer

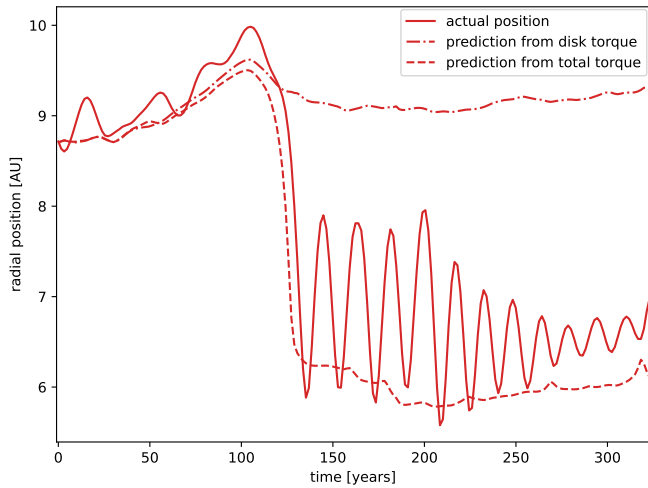


Figure 5. Evolution of the radial position of clump MCA-4 during the interaction with MCA-3. The clump (solid line) is pulled inward during the interaction and continues on an eccentric orbit. The position can only be correctly predicted by taking into account the clump-clump interactions, implying that the rapid change in radial position is caused by the latter.

Lindblad resonance causes a negative torque. However, we note that a direct comparison with linear torque theory would not be well-posed since the gas flow in gravitationally unstable discs is turbulent and there is no well-defined background flow, rendering any perturbative treatment meaningless. In the following sections we discuss the effect of the different components in more detail.

3.3 Clump-clump interactions

A potentially important component of the torque which is usually not present in conventional models in which migration is treated as a pure planet-disc interaction are clump-clump interactions (see also [Boss \(2013\)](#); [Boss \(2023\)](#)). An example of such an interaction is shown in [fig. 5](#). It shows the radial position of clump MCA-4 over time. The solid line shows the radial position of the clump in the simulation. At a time of ~ 120 yr, the clump suddenly moves inward on an orbital timescale. The orbital time of the clump is reduced from ~ 25 yr to ~ 15 yr. The two other lines in [fig. 5](#) show the position predicted from the torque using the procedure outlined in [section 2.3](#). The dashed line which shows the predicted position taking into account the total torque closely follows the actual position of the clump. It is not exact which is likely due to the fact we only use the simulation data in snapshots with discrete spaces of $10/2\pi$ yr and that we assumed zero eccentricity. The plot also shows the dash-dotted line which is the predicted position from the disc torque, meaning all torque components except for clump-clump interactions. It can be seen that from the point on where the clump begins to move inward, the disc torque predicts an almost constant radial position of the clump. This shows that this rapid inward migration is really due to clump-clump interactions.

The situation is shown in the density plots in [fig. 6](#) showing the inner part of the disc at successive times. The clump MCA-4 which is migrating inward and another close-by clump MCA-3 are marked with the red circles. It can be seen that the clump MCA-3 (being on a faster orbit) approaches MCA-4 and thereby scatters it inward. The orbit of MCA-3 is less influenced as it is a more massive clump.

Besides the fast inward migration, gravitational scattering also leads to a more eccentric orbit as can be seen in the oscillating

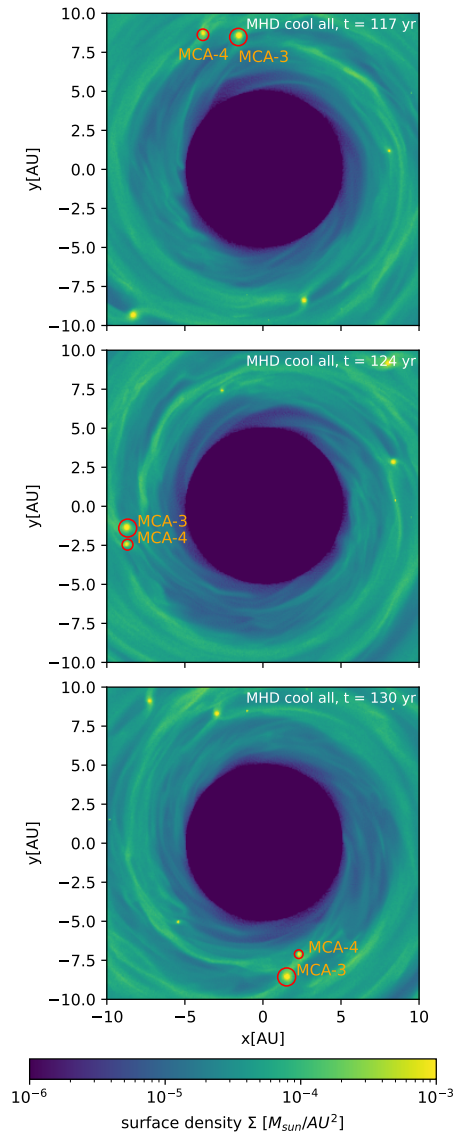


Figure 6. Surface density plots of the disc during the interaction of clump MCA-4 with MCA-3. The more massive clump MCA-3 approaches the clump MCA-4 from the back which is deflected inward and continues on an eccentric orbit.

behaviour of the radial position in [fig. 5](#). The eccentricity of the orbit is plotted in [fig. 7](#) (bottom right). This is measured by evaluating the specific energy ϵ and the specific angular momentum l of the clump and then using

$$e = \sqrt{1 + 2\epsilon l^2 / (M_{\text{star}}^2 G^2)}. \quad (7)$$

It can be seen that around the time of interaction, the eccentricity increases significantly. However during a time of 100 yr the orbit circularizes again. This can be due to the interactions with the gas disc, or subsequent weaker interactions with other clumps but the fact that clump-clump interactions don't seem to increase the eccentricity over the long term (bottom plots in [fig. 7](#)), suggests that the circularization is caused mainly by the interaction with the disc. This result suggests that although clump-clump interactions may lead to an increase in eccentricity of the clumps, one may still expect on average low-eccentricity orbits ($e = 0.1 - 0.2$) as the eccentricity can quickly diminish again. We note that the values of the eccentricity

found in these simulations are similar between magnetized and non-magnetized discs, and are in agreement with earlier results in the literature (e.g. Mayer et al. (2002, 2004)).

Fig. 7 shows the action of the clump-clump torque. For four clumps it shows the torque strength over time (top) and the radial position of the clump (solid line, bottom) together with the predicted position of the clump taking into account only the clump-clump torque (dashed line, bottom). It can be seen in the top part of the figure that the clump-clump torque acts on a short timescale and often switches the sign periodically. This is due to the clump overtaking / being overtaken by another clump on a close orbit and thus the direction of the gravitational force exerted from the other clump switches. In the bottom of fig. 7 it can be seen that this leads to fast, almost discrete changes in the predicted radial position of the clump. The magnitude of the clump-clump torque and thus its importance relative to the other components of the torque differs much between the clumps: in the case of clump MCA-4 the effect of the clump-clump interactions dominate over other components of the torque; in MCA-2 and MCA-3 both are important and in MCA-1 clump-clump interactions are only of minor importance.

Fig. 8 quantifies the overall importance of the clump-clump torque taking into account the different runs. It compares the migrated distance of each clump over the simulation to the distance it would have migrated if the disc torque alone would have interacted with it. The clumps of different runs are marked with different symbols, the clumps in blue, orange, green and red are the ones we show in the grid plots for each run. The dashed line is the identity, clumps on this line did not experience an overall change in their radial position due to clump-clump interactions. This is also the region where most of the clumps are in the plot. However especially in the *MHD cool-all* case there are some clumps that are far away from the line and for which the disc torque yields a secondary contribution. Deviations from the line occur both from above and from below, signaling that clump-clump interactions can lead to both a positive and a negative torque, and thus contribute to both inward and outward migration. Overall, we infer that clump-clump interactions add a degree of randomness to the dynamics of the system which, in some instances, and for a limited time span, can affect significantly the dynamics of the clumps.

Nevertheless, in the *MHD cool disc* and the *HD* case however, the disc-driven torque is the most important component. This is presumably because both runs have a lower number of clumps compared to the *MHD cool all* simulations, thus reducing the occurrence of clump-clump interactions and also because of the higher masses in the *MHD cool all* run. In the next section we analyze and discuss the role of the disc-driven torque in migration at greater depth.

3.4 Decomposition of the disc torque

In this section we attempt to determine to what extent the orbital evolution of the clumps, and thus the time-integrated effect of the torque, can be or can not be reproduced by considering only a subset of the disc torque components, and neglecting the episodic effect of clump-clump interactions. We should note that, in principle, even when clump-clump encounters are negligible, multiple clumps are always present in the disc and might perturb the orbit of a given target clump because of their long-range gravitational effect. We quantify the role of such “far-field” perturbations by analyzing the radial profile of the torque acting on several target clumps. We perform the analysis for different clumps and at different times, but show the results for only one representative time in this paper, in fig. 9, since we found the result to be similar in the various cases considered. We

compute the profiles by dividing the disc into 100 radial bins. For each fluid element in the system we then calculate in which bin it lies and add its contribution to the torque to the corresponding bin. Fig. 9 shows that usually the dominant torque component originates from disc material relatively close to the target clump, which does not correlate with the location of other clumps. The latter, especially in the magnetized runs (see the panels for “MCA-” clumps in the figure) clearly produce both positive and negative torque components, as there are bumps correlated with their locations. The amplitude of these bumps is usually much lower than that of the dominant torque component in the co-orbital region around the target clump. When torque peaks appear near clumps, they are transients, as seen by comparing fig. 9 to fig. A2 in two adjacent time-steps (see e.g. clump MCA-1). Instead, the high amplitude torque, negative or positive, in the co-orbital region, is a robust feature, both in the HD and in the MHD runs. Additionally, we do not notice systematic differences in the torque profiles between MHD and HD runs, rather the specific dynamical state of the system, especially the perturbations induced by other clumps, is what determines, at any given time, the shape of the torque profiles.

In fig. 9 we also show the location of the low-order Lindblad resonances, which, in standard Type I migration, are the locations where the exchange of angular momentum with the disc is maximal and the torque is stronger. Clearly there are no significant features in the torque profiles associated with these resonance in our simulations. The rare instances in which a prominent torque feature is seen at a similar location are mostly associated with a perturbing clump. We also note that the dominant torque does not come from material at Lindblad resonances, thereby highlighting how the nature of disc torques in self-gravitating, fragmenting discs is different from classical Type I migration in low-mass, non-self-gravitating discs. The local nature of the torque in self-gravitating discs was pointed out also by Malik et al. (2015), who studied individual migrating protoplanets in marginally unstable but smooth (non-fragmenting) discs using a very different hydrodynamical code, the finite-difference polar grid code FARGO-ADSG (Masset 2000; Baruteau & Masset 2008b), which solved the fluid equations in the co-rotating frame and in two dimensions.

We now consider the effect of the different components of the disc torque over time, rather than at fixed time, and divide them into three different components as described in section 2.3: inner disc torque, outer disc torque, and a torque from within one Hill radius around the respective clump’s orbit. In order to compute these components, we first determine for each fluid element if it is part of another clump. In that case we don’t count it here and it only contributes to the clump-clump torque. We then determine in which region the fluid element lies: if its orbit is at a distance within a Hill radius around the clump’s orbit we count it towards the “Hill torque”. If the fluid element is on an orbit further than a Hill radius of the clump’s orbit it counts either to the outer or the inner torque depending on if it is inside or outside the clump’s orbit. The contribution due to each component is then determined by summing the gravitational torques from each fluid element belonging to that component. We further compute the torque from within 2 Hill radii around the respective clump’s orbit (see section 2.3). We note that this component overlaps with the outer / inner disc torques.

In fig. 10 we show the effects of the inner and outer disc torques and compare them to the effect of the (total) disc torque and to the actual migration of the clumps. First it can be seen that the for most clumps the outer disc torque (dotted lines) is negative and therefore its isolated effect is an inward migration of the clump. Conversely, the inner disc torque (dashed lines) is mostly positive and therefore leads to outward migration. This is analogous to the Type I picture where

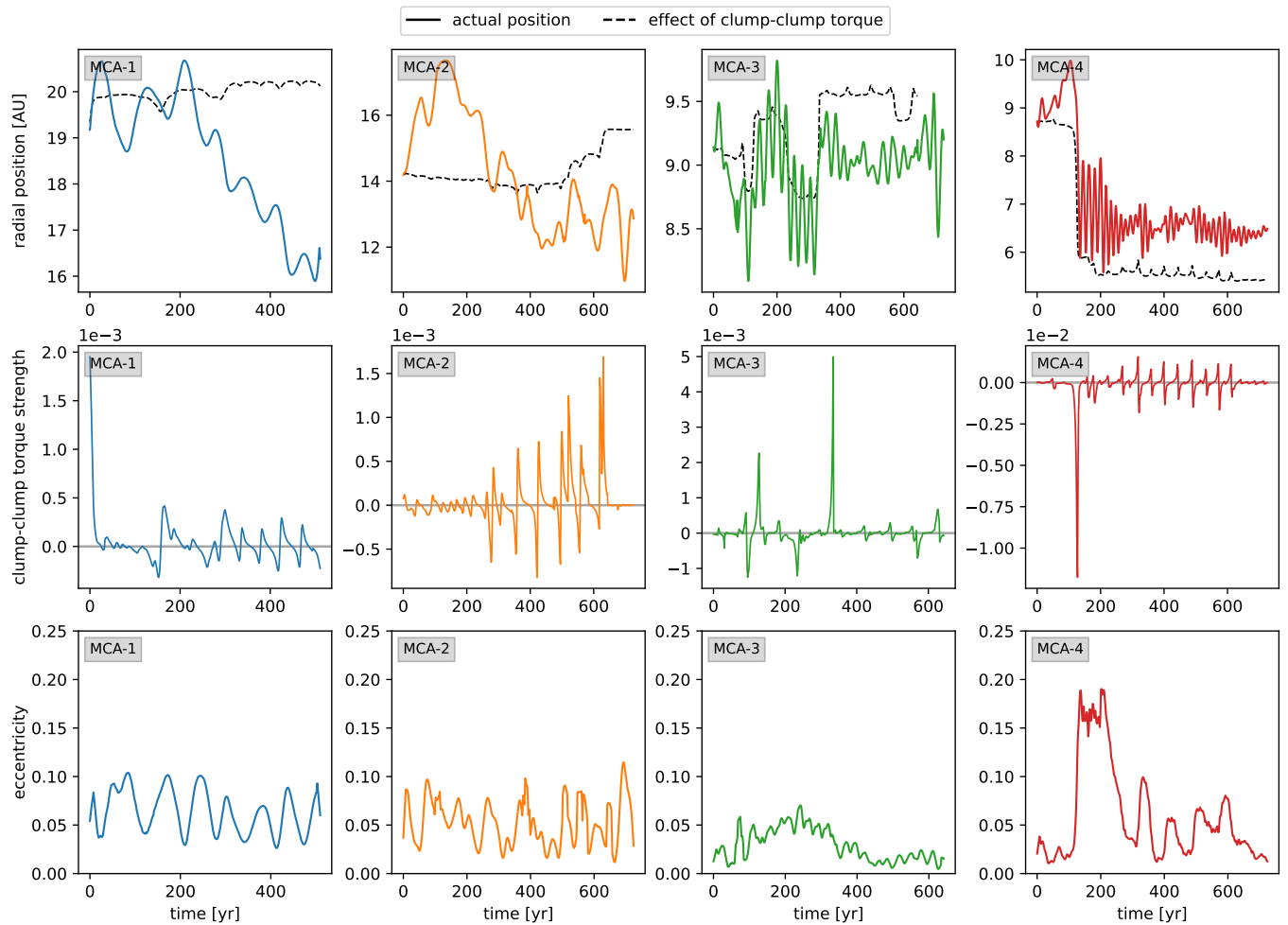


Figure 7. The clump-clump torque for the *MHD cool all* case. Top: radial position of the clumps (coloured solid lines) and predicted positions taking into account only the effect of the clump-clump torque (black dashed line). Middle: torque strength arising from clump-clump interaction for four different clumps. Bottom: eccentricity evolutions of the clumps. The clump-clump torque consists of short spikes leading to fast changes in the radial positions compatible with the short time of close-by encounters. Except for clump MCA-4 the clump torque alone does not seem to be the main driver of migration. Further, clump-clump interactions do not seem to lead to highly eccentric orbits on the long-term.

the OLR and ILR cause torques in opposite directions. In the plot we also show the sum of these two contributions (dash-dotted lines). It can be compared to the effect of the (total) disc torque (black solid line). Overall these parts of the torque are not in a good alignment with the total disc torque (except for MCA-3) hinting towards a greater importance of the material on orbits close to the clump.

Therefore we now focus on the torque components near the clump’s orbit. Also the radial torque profiles in fig. 9 suggest that these parts are most often the dominant contributions; apart from clump-clump interactions. This may come from the gas flowing asymmetrically through the clump’s orbit as well as by material in the circumplanetary disc assembling around the clumps (Szulágyi et al. 2016). For migrating planets in non-self-gravitating discs it has been shown that fast, Type III migration takes place. This is driven by the gas flowing through the horseshoe region, which yields a negative torque, which can be compensated, or not, by a positive torque induced by material in the circumplanetary disc (Masset & Papaloizou 2003b; Papaloizou et al. 2007). If the mass flowing through the horseshoe region is larger than the sum of the masses of the protoplanet and circumplanetary disc, then this so-called “mass deficit” gives rise to a net negative torque and the fastest mode of Type III migration,

called runaway migration, arises. For individual migrating protoplanets in massive self-gravitating discs, it has been shown that the conditions for runaway migration are naturally satisfied (Malik et al. 2015). If, temporarily, the mass deficit becomes negative, then the positive torque induced by the circumplanetary disc material can, in principle, generate outward migration.

In our analysis we find that considering the contribution of the material within 2 Hill radii which we defined as

$$r_{\text{hill}} = r \sqrt[3]{m/m_{\text{star}}}, \quad (8)$$

with m the mass of the clump and r its radial position, neatly identifies the region mostly responsible for the disc torque. When comparing the torque induced by the material within twice the Hill sphere with the total disc torque, we find that the former provides the most important contribution to the orbital evolution of the clumps, as shown in fig. 11 by the fact that it best reproduces the clumps’ radial distance evolution overall. We stress that this is true both for inward and outward migrating clumps.

Fig. 12 shows that the total migrated distance of each clump is very well reproduced by considering only this torque component. For most of the clumps, already the torque from within 1 Hill radius

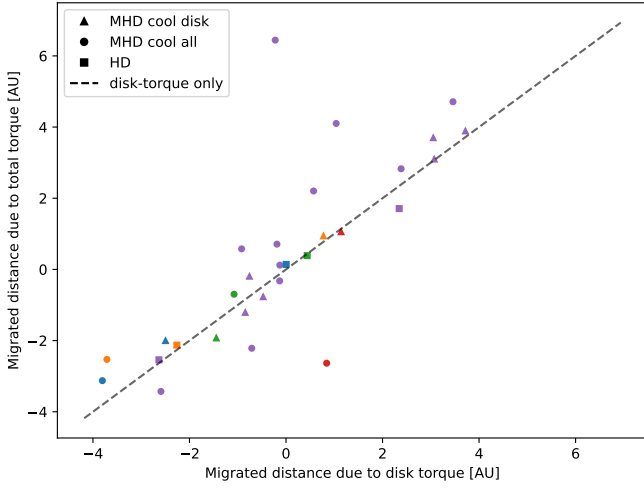


Figure 8. Migrated distance due to the total torque vs migrated distance due to the disk torque for each clump of the three runs. Deviations from the diagonal line signalize situations in which clump-clump interactions can not be neglected in explaining the clump’s migration. For most clumps the disk torque is more important, however for some clumps especially in the *MHD cool all* run, the clump-clump interactions dominate, as shown by the larger deviations of the corresponding data points with respect to the diagonal line.

around the clumps’ orbits reproduces the (total) disc torque contribution quite well. The results are also in excellent agreement with the findings of 3D SPH simulations of migrating black hole perturbers in self-gravitating circumnuclear discs in galactic nuclei (Mayer 2013; Souza Lima et al. 2020), suggesting that the local nature of the torque is a general property of this regime. Note that in the latter works, as in Malik et al. (2015), perturbers were evolving in a marginally unstable but non-fragmenting disc, hence torques were only generated by the surrounding disc. In our case, as we have extensively shown, clump-clump encounters and perturbations also play a role.

Fig. 13 shows different timescales relevant for migration and compares them to the actually measured migration time. We first calculate for each clump the mean migration rate by measuring $s = \langle |\dot{r}_p/r_p| \rangle$ where r is the clump’s radial position. The average is taken over each snapshot of the simulation. We take the absolute value of the term in the brackets because we have both in- and outward migration. The migration time is then $t_{\text{mig}} = 1/s$. We then use this time as a reference for the other timescales.

We calculate the Type I Lindblad torque from Paardekooper et al. (2010):

$$\Gamma = \Gamma_0/\gamma (-2.5 - 1.7\beta + 0.1\alpha), \quad (9)$$

with

$$\Gamma_0 = \frac{m^2}{m_{\text{star}}^2 h(r_p)^2} \Sigma(r_p) r_p^4 \Omega(r_p)^2. \quad (10)$$

Here, α and β are the negative power-law exponents of the surface density profile ($\Sigma \propto r^{-\alpha}$) and the temperature profile ($T \propto r^{-\beta}$), $\gamma = 5/3$ is the adiabatic index, m the mass of the clump, m_{star} the mass of the central star, h the aspect ratio of the disc, Ω the angular velocity of the disc and r_p the radial position of the planet. It can be seen that for most clumps the Type I Lindblad migration timescale t_{T1} is ≈ 10 times more than t_{mig} , for some clumps much more. Further, the Lindblad torque does not predict the correct direction of migration. This is already expected from our results as we showed

that most of the contribution comes from material on orbits close to the clump.

We also estimate the viscous timescale by

$$t_{\text{visc}} = \frac{r_p^2}{\alpha c_s h}, \quad (11)$$

with α the viscous stress; in this case (since there is no viscosity in the simulation) an effective value coming from gravitational, Reynolds and Maxwell stresses. In our case $\alpha \approx 0.2$ for the magnetized runs and $\alpha \approx 0.1$ for the unmagnetized run (Deng et al. 2020). The variable c_s is the sound speed of the disc. It can also be seen that for most clumps t_{visc} is ≈ 10 times longer than the migration time, thereby also ruling out Type II migration (Lin & Papaloizou 1986b; Cloutier & Lin 2013) through gap-opening.

We finally compute the libration timescale (Baruteau & Masset 2008a)

$$t_{\text{lib}} = \frac{8\pi r_p}{3\Omega r_{\text{hs}}}, \quad (12)$$

with $r_{\text{hs}} \approx 2.5r_{\text{hill}}$ (Paardekooper & Papaloizou 2009) the width of the horseshoe. It can be seen that for many clumps t_{lib} is of the same order as the migration time and for many clumps it is much shorter which means that the observed migration is consistent with fast Type III migration similar to what was observed in Malik et al. (2015).

We caution that, despite the apparent consistency with the Type III migration scenario, the flow dynamics in fragmenting discs is not only very different from the conditions in conventional simulations for migrating planets in non-self-gravitating discs, but also different from the conditions in self-gravitating but non-fragmenting discs such as in Malik et al. (2015). During fragmentation the gravitational stress is maximal (Lodato & Rice 2004; Deng et al. 2020), hence the departures from the axisymmetric Keplerian flow are the largest possible, with significant spatially and time-varying local radial motions. As a result, one expects the migration rate to fluctuate. We therefore neither expect monotonic runaway migration (as often documented in the literature for non-self-gravitating discs for the first ≈ 20 orbits (Peplinski 2008)), nor saturated steady state migration. Finally, fig. 14 shows the second derivative of the clumps’ radial positions (acceleration of migration), for representative cases. In the case of runaway migration, one would observe a monotonic and possibly exponential increase of acceleration; whereas in a steady state migration, the acceleration would vanish. Instead, the second derivatives of our clumps are fluctuating quickly, often changing sign on an orbital time. In the next section we discuss this point further.

4 DISCUSSION AND CONCLUSIONS

We investigated planetary migration in self-gravitating and also magnetized discs. To this end, we analyzed high-resolution simulations in which protoplanetary clumps formed through fragmentation, both in presence or absence of a magnetic field. We intentionally refrained from employing sink particles for the clumps to avoid spurious numerical effects.

For our analysis we computed the gravitational torque exerted on the clumps in discrete snapshots and computed a predicted radial position in each snapshot. This method showed good agreement with the actual radial position of the clumps. We then dissected the torque into multiple components in order to associate the radial evolution of the clumps with effects due to different components of the surrounding flow. In particular, we separated the torque due to clump-clump collisions from that due to the disc.

Our main results can be summarized as follows:

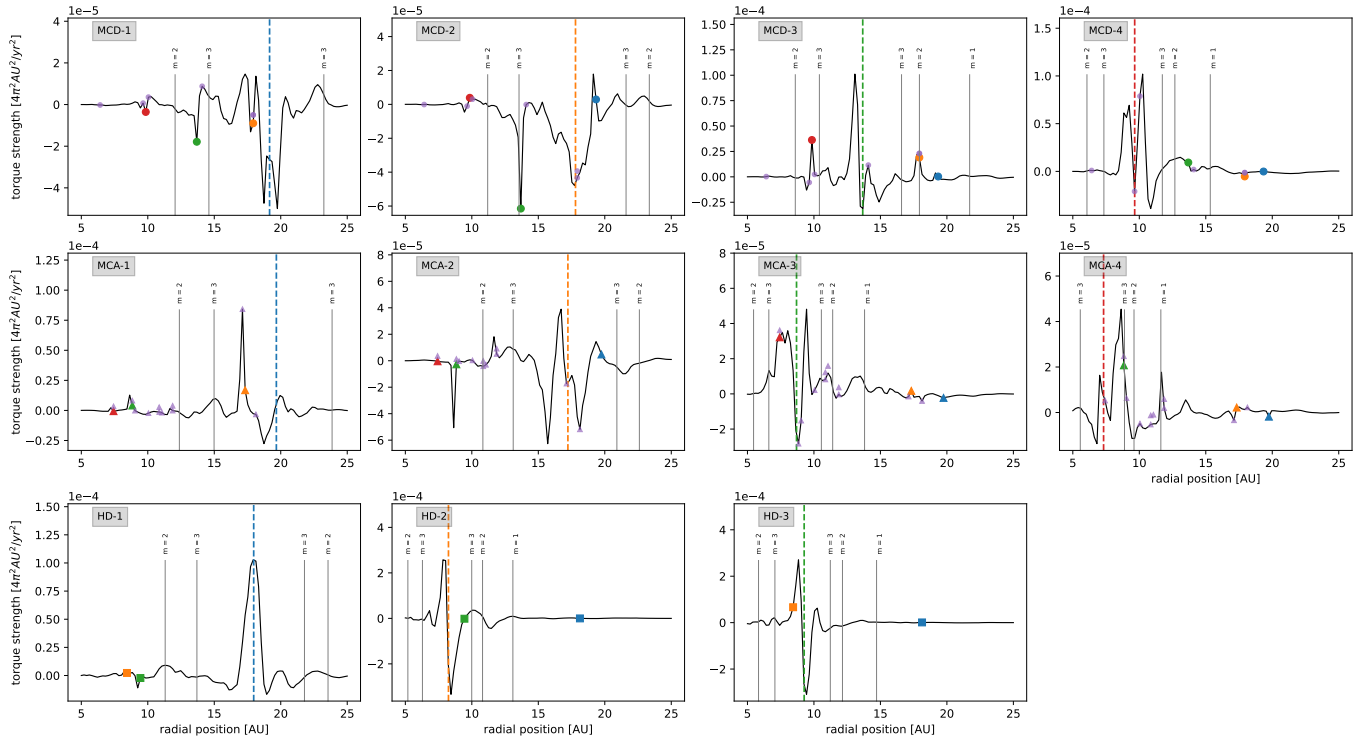


Figure 9. Profiles of the torque acting on each clump at time $t \sim 160$ yr. The y-axis shows the torque strength and the x-axis shows the radial position in the disc, revealing where the torque is coming from. The position of the respective clump is shown with the dashed lines and the radial positions of the other clumps are shown with the coloured dots. The position of the lowest Lindblad resonances are shown with the labelled, thin grey lines.

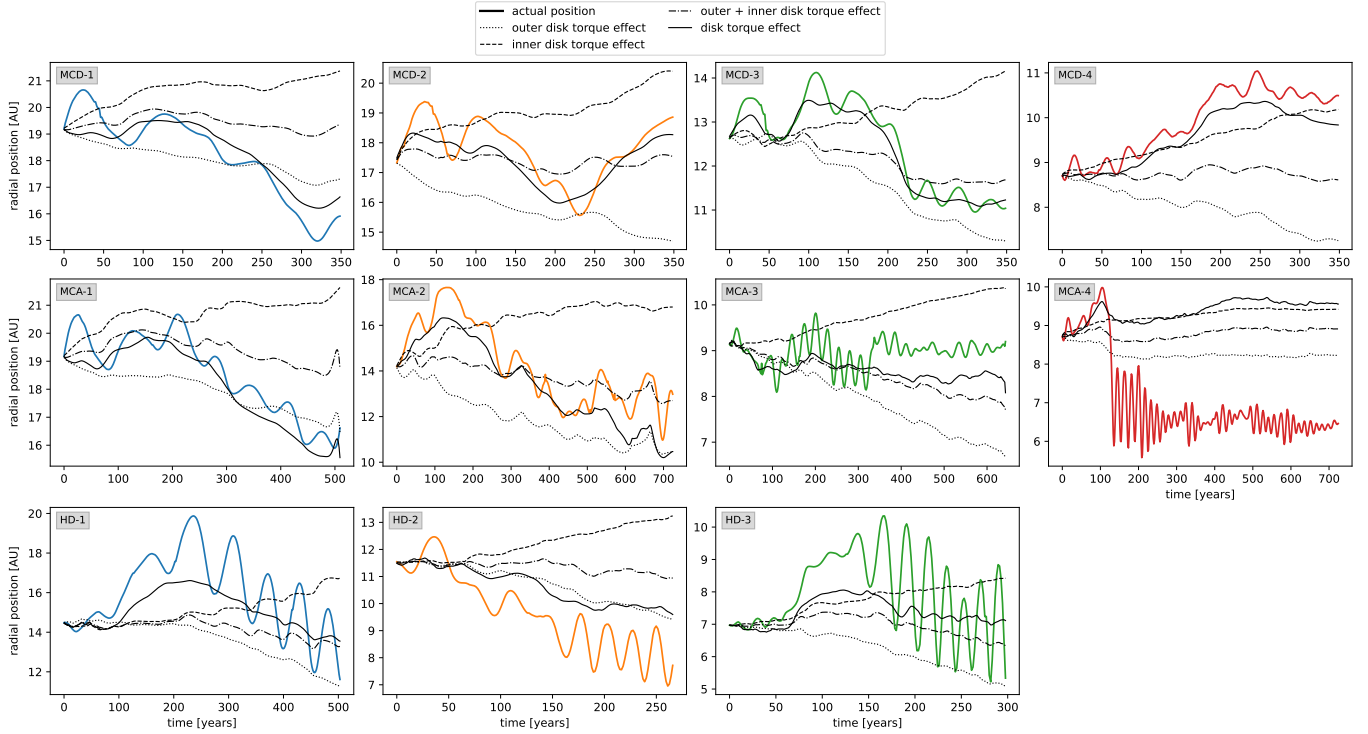


Figure 10. Comparison of the effects of the inner and the outer disc torque for different clumps. The evolution of the actual radial position of the clumps is represented by the coloured solid line. The outer disc torque (dotted line) tends to pull the clumps inward whereas the inner disc torque (dashed line) pulls them outward. Together (dash-dotted line) these two torques are for some clumps in alignment with the total effect of the disc torque (black solid line), however the torque from $2r_{\text{hill}}$ shown in fig. 11 resembles the evolution of the clump's radial position much more closely.

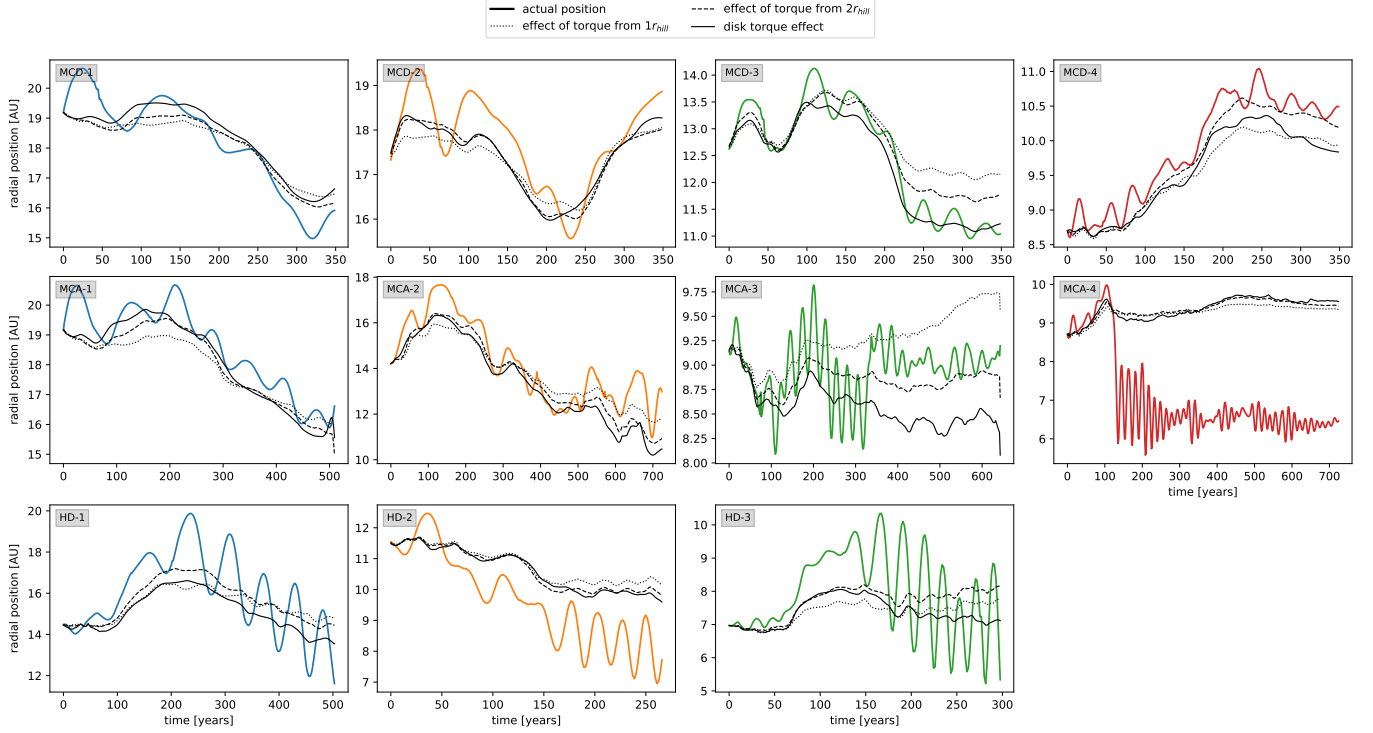


Figure 11. Comparison of the effects of the torque from up to $1r_{\text{hill}}$ (dotted line) around the orbit of each clump and the respective torque from up to $2r_{\text{hill}}$ (dashed line; contains the former) to the total disc torque representing the total torque without clump-clump interactions (dash-dotted line, contains the former two). The evolution of the actual radial position of the clumps is represented by the solid line. The torque from $2r_{\text{hill}}$ seems to account for most of the migration when neglecting clump-clump interactions and the other components of the disc torque (outer and inner disc torque) are only occasionally important.

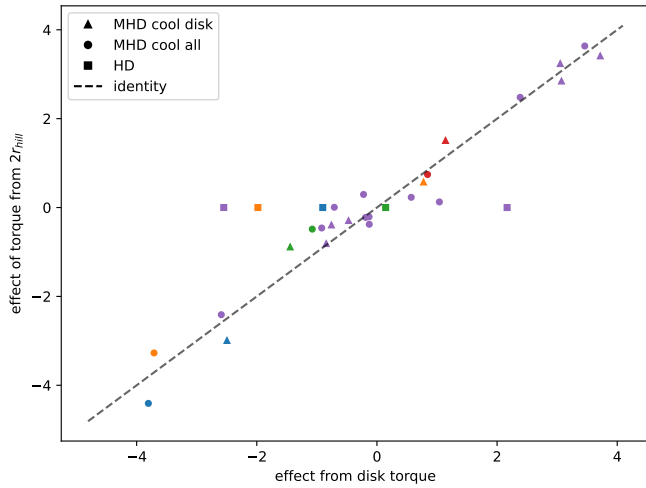


Figure 12. The y-axis shows the migrated distance due to the torque arising from the matter on orbits of at most two hill radii apart from the clump’s orbit; the x-axis shows the migrated distance due to the disc torque for each clump. Most of the disc torque can be explained by the “ $2r_{\text{hill}}$ ” torque, shown by the fact that most clumps lie close to the diagonal line.

- Clump-clump interactions add stochastic perturbations to the radial evolution of the clumps, but for most clumps they are less important than the disc-driven torque. Only in the *MHD-cool-all* run, they are of comparable importance to the disc torque, probably due to higher clump masses. In the *HD* runs, there are fewer clumps, hence clump-clump interactions are less frequent despite of the masses being on the higher end. We note that the clump-clump interactions

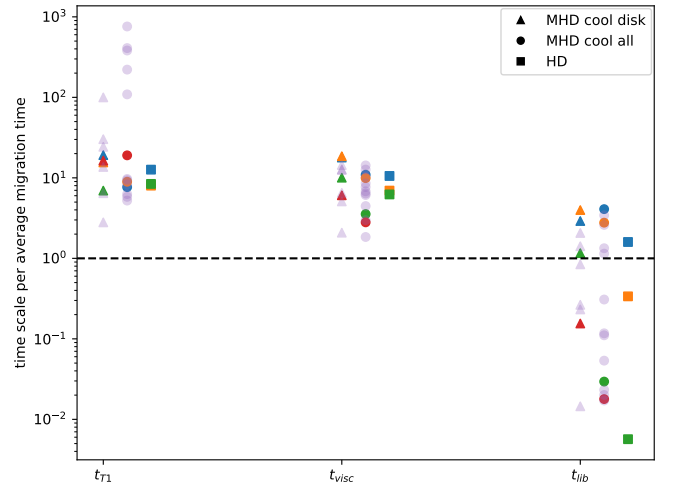


Figure 13. Comparison of different timescales relative to the measured migration time. For most clumps the Type I (Lindblad) migration timescale t_{T1} and the viscous timescale t_{visc} (Type II migration) is much longer than the migration time. Only Type III migration, is compatible with the observation as the libration timescale is similar or shorter than the migration timescale.

occurring in the simulations excite the eccentricity only very briefly, hence they do not lead to higher eccentricities on orbital timescales.

- The disc torque impacting the clumps has an inner disc component which yields a positive contribution, and an outer component which yields a negative contribution. This is true for most of the clumps, and resembles qualitatively the behaviour of the torque in Type I migration, although in our case the amplitude of the torque is

not due to the resonant interaction with the disc; rather it is dominated by a local contribution.

- The torque contribution arising from material on orbits of at most $2r_{\text{hill}}$ away from the clump’s orbit is enough to essentially explain the orbital evolution of the clumps due to disc-driven torques (neglecting clump-clump interactions). This suggests the development of a new prescription for migration of protoplanetary clumps to be used in population synthesis models of disc instability planets (e.g. (Müller et al. 2018; Forgan et al. 2017; Schib et al. 2023)). This will be the subject of future work.

- The nature of disc-driven torques is the same in magnetized and unmagnetized discs, being controlled by the gravitational effect of the local gas flow. This is true despite the significant difference in clump masses in MHD versus HD runs, the former being 1-2 orders of magnitude less massive and thus migrating slower.

- The timescales of migration for each clump are faster than what would be expected from Type I migration and also faster than the viscous timescale, ruling out Type II migration. In confirmation of this, we do not observe fully developed gaps along the clump’s orbits although the most massive clumps in the *MHD cool all* case seem to open partial gaps, that do not extend around the full azimuth. Both the large turbulent viscosity and the fast migration timescale are likely responsible for the stifling of gap opening. Instead, the libration timescales are comparable or shorter than the migration timescale, consistent with Type III migration.

The eccentricities of the clumps measured in our simulations are ≈ 0.1 and not much influenced by clump-clump interactions over the long term. This is even true for the two mergers we observed in the *MHD cool all* run. They lead neither to a strong increase in eccentricity nor in inclination of the orbits. This is probably because the respective clumps were almost co-planar, with an angle between their angular momentum vectors of $\approx 1^\circ$. Matzkevich et al. (2024) simulated colliding clumps that formed through disc instability, without including the surrounding disc but exploring a wide parameter space in terms of orbital configurations and clump masses. Although they observed perfect mergers, whereby the mass of the new protoplanet corresponds to the sum of the colliding bodies (which also roughly holds for our mergers), such events were rare. However, their masses were considerably larger than ours, ranging from 3–10 M_{Jup} ; while the upper end of the mass range was more stable against disruptions from collisions. They found that while even collisions with impact velocity v_{imp} below the mutual escape velocity v_{esc} of the clumps could result in substantial mass loss or trigger dynamic collapse, $v_{\text{imp}} \lesssim v_{\text{esc}}$ was found to be a necessary condition for perfect merging. This condition is also fulfilled in the (perfect) mergers observed in our simulations.

The consistency in the nature of the disc-driven torque between the MHD and the HD runs is not a trivial result since the former have been shown to be significantly more turbulent, having an effective “alpha” viscosity as high as 0.2 – 0.4 due to a combination of the gravitational and Maxwell stress (see Deng et al. (2020)). Turbulent diffusion is known to play a role in the saturation of the horseshoe drag in non-self-gravitating discs (Baruteau & Lin 2010). Equivalently, here turbulent diffusion could impact the amplitude of the dominant local torque component by maintaining a sufficiently high mass flow near the Hill sphere. In that respect, the HD and MHD runs might behave similarly because the effective viscosity is different between the two but only by factors of 2-3.

A high mass diffusion rate through the Hill sphere likely plays a key role in causing a Type III-like migration behaviour by keeping the co-orbital torque unsaturated. In conventional Type III migration studies,

which are carried out in non-turbulent discs, it has been shown that the fastest form of Type III migration, runaway migration, does not occur, rather the acceleration saturates after an initial increase (Peplinski 2008). Here we have shown (see section 4) that the acceleration does not have a monotonic evolution, rather it is highly fluctuating. This underpins how the relevant regime is only superficially akin to the Type III migration mode described in the literature. Instead, our results suggest that our migration regime, even in absence of clump-clump interaction, is highly stochastic.

The stochasticity of migration observed in our simulations reflects the gravito-magneto-turbulent regime of the flow (with only gravito-turbulence in absence of the magnetic field). In Wu et al. (2024), who studied migration of low-mass planets, it was found that for a highly turbulent flow, chaotic migration dominates over classical Type I migration. They determined a critical transition mass for the planet to undergo chaotic migration, around $q \lesssim \lambda a h^3$ where q is the planet to star mass ratio. The factor λ was determined to be $4 < \lambda < 25$ (Wu et al. 2024). In the case of our discs, the critical limit would be in the range of $0.05 < q_{\text{crit}} < 0.3$. Therefore, chaotic migration is compatible with the conditions in our simulations.

Our simulations allow to study the effect of clump-clump interactions but we did not observe any ejections of clumps. Such ejections have been previously observed in simulations with sink particles (Boss 2023) and could be related to the free-floating planets, observed e.g. in Miret-Roig et al. (2022). It is important to realize that the ineffectiveness of clump-clump collisions in scattering protoplanets out of the disc, a major result of our work, might be in part due to the limited spatial resolution. Indeed, since the clump sizes can not shrink below the gravitational softening of 0.05 AU, collisions remain forcefully soft, which could underestimate the exchange of kinetic energy and angular momentum between clumps, thereby suppressing ejections artificially. However, previous one-dimensional collapse models as well as 3-dimensional hydrodynamical simulations of individual collapsing clumps (Helled & Schubert 2008; Galvagni et al. 2012; Helled et al. 2014) have computed characteristic pre-collapse timescales, defined as the time required for the clump to become dense and hot enough to reach molecular hydrogen dissociation, after which a much faster dynamical collapse to planetary sizes would follow. Pre-collapse timescales range from a few 1000 to a few 10^5 yr for clumps of 1-10 Jupiter masses with solar metallicity and filled with interstellar-size grains, with the shortest timescales holding for the upper end of this mass range. The clumps in our simulation reach a maximal mass of the order of a Jupiter mass, but some may grow further in the *MHD cool all* case. If that is the case, they would collapse much faster than the lifetime of the disc, leading to a later evolutionary phase where clump-clump interactions could become much stronger due to the smaller sizes of the clumps—a regime we have not covered in our simulations. However, for the Jupiter-mass clumps, which we actually observe in our simulation, the pre-collapse timescales are comparable to the disc lifetime, hence clump-clump collisions would be as soft as modelled in our simulations. In the *MHD cool disc* run, which is probably more realistic as it accounts for the clumps’ interiors being optically thick (see section 2.2), the clumps do not reach Jupiter masses. For the Neptune-mass clumps observed in our magnetized runs an even longer pre-collapse phase is expected. In further support of this statement, preliminary work using 1D collapse calculations similar to those of Helled & Schubert (2008) but starting with the clump’s density and temperature occurring in our simulations (Kubli et al., in prep.), show that collapse timescales typically exceed a few 10^6 yr for clumps below Saturn masses, even for higher than solar metallicities.

We can estimate directly the effect of clump compactness on the

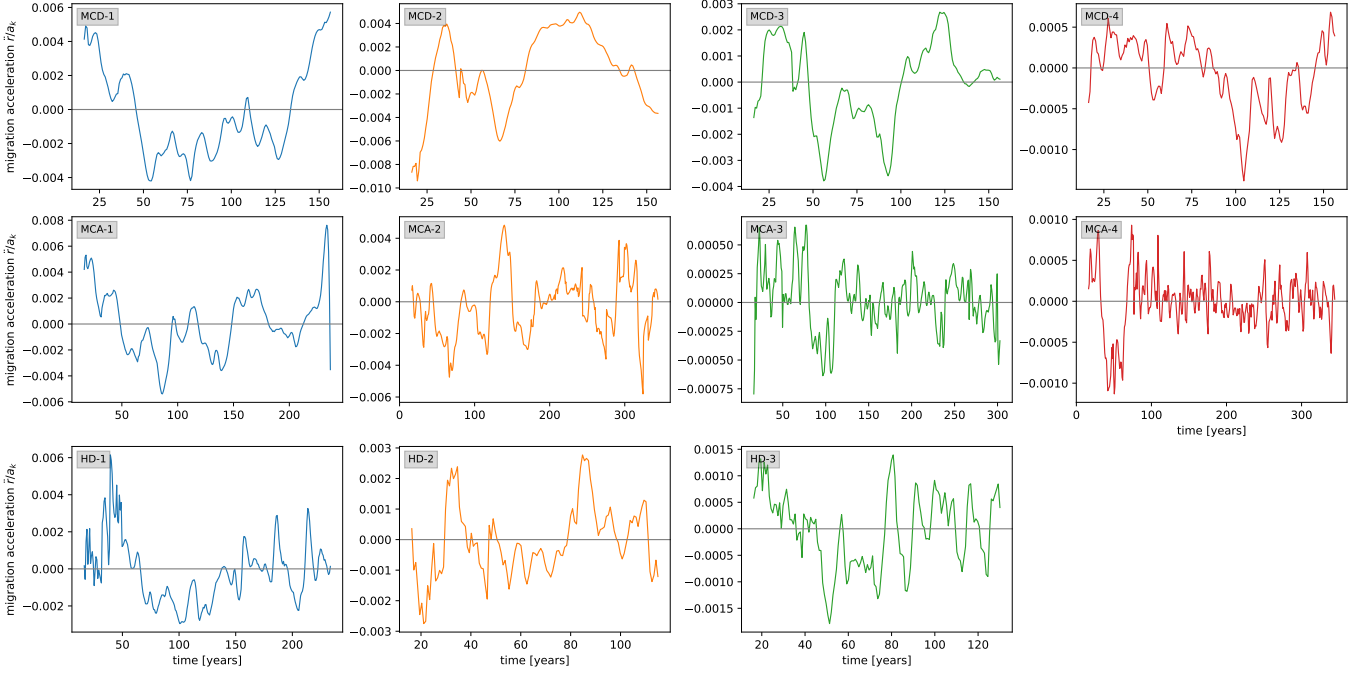


Figure 14. Acceleration of the radial migration for a representative subset of the clumps. The acceleration is normalized to the Keplerian orbital acceleration and smoothed over ≈ 60 yr corresponding to an orbital time at 15 AU. For most clumps, the sign of the acceleration is alternating appreciably, in line with the stochastic migration scenario.

relative velocity of the clumps. As mentioned above, the mutual gravitational acceleration of the two interacting clumps will increase with decreasing impact parameter, and more compact clumps can encounter one another with smaller impact parameters. We can estimate the impact parameter below which the relative velocity of the clumps becomes comparable to the Keplerian orbital velocity. Computing $d_{\min} = 2G(m_1 + m_2)/v_{\text{Kepler}}^2$ yields values of 40 – 400 times smaller (for $0.5M_{\text{Jup}} - 0.01M_{\text{Jup}}$) than the sizes of our clumps. This implies that protoplanets would have to collapse by more than an order of magnitude in order for ejections to occur in the inner disc region, where the clumps form in our simulations. Due to the long collapse timescales, such a compact configuration is only relevant at a much later evolutionary stage compared to the timescales probed by our simulations, confirming the robustness of our findings.

A caveat is that additional mechanisms such as pre-enrichment, grain growth to pebble sizes and grain sedimentation, would all concur to reduce opacities, especially at metallicities higher than solar. Helled & Bodenheimer (2011) have shown that the opacity reduction can decrease the pre-collapse timescales by up to two orders of magnitude. Nevertheless, even with such an acceleration of the pre-collapse stage, the Neptune-sized clumps in our MHD simulations would still evolve slowly enough to remain diffuse and undergo soft collisions over the short timescales probed by our simulations. The interplay between contraction timescales and dynamics will have to be investigated in the future. As already mentioned, Matzkevich et al. (2024) found that clump-clump collisions can trigger fast collapse under certain conditions, especially for older, evolved clumps. In the latter case though, the collapse would occur after perfect merging, hence no ejection would occur.

The inability of clump-clump collisions to eject protoplanets can also depend on where in the disc these collisions occur. Our discs

are relatively compact, hence by construction there are no encounters occurring beyond 20-25 AU. We can then ask at what distance from the centre, given a more extended disc, clump-clump collisions with properties as those in our simulations, would lead to ejection. This will happen when the kinetic energy transferred in the collision becomes larger than the clump’s binding energy to the central star. Equivalently, one can compare the relative velocity in the collision with the local Keplerian velocity. For this purpose we measured the relative velocity of clump pairs undergoing a close encounter. In the case presented in fig. 5, when they are at closest distance to each other, their relative velocity is 0.35 AU/yr, whereas the Keplerian velocity at their position is 2.12 AU/yr. Similar values are found for other close encounters. The measured relative velocity would correspond to the Keplerian velocity at a radial distance of ≈ 300 AU for the same disc mass and stellar mass. Of course this distance could be somewhat smaller in discs around lower mass stars, but only by a small factor.

Overall, our findings in the simulations combined with the arguments just outlined lead us to conclude that ejections should be a rare phenomenon in protoplanetary discs undergoing fragmentation, thereby not yielding a significant contribution to the population of free-floating planets. These could be produced via other mechanisms, involving still some form of gravitational collapse in the gas phase triggered by other phenomena, for example as a result of tidal interactions of protoplanetary discs (Fu et al. 2025). Instead, fast, stochastic migration is the distinctive phenomenon governing the evolution of orbits of clumps arising in disc instability.

ACKNOWLEDGEMENTS

We thank Christian Reinhardt for interesting discussions and helpful comments. This work is supported by the Swiss Platform for Advanced Scientific Computing (PASC) project SPH-EXA2 and by NCCR PlanetS. We also thank the Swiss National Supercomputing Center (CSCS) where the simulations were carried out on the PizDaint and Eiger supercomputers on the "uzh3" rolling account.

DATA AVAILABILITY

The data files that support our analysis will be made available upon reasonable request.

REFERENCES

- Baruteau C., Lin D. N. C., 2010, *ApJ*, 709, 759
- Baruteau C., Masset F., 2008a, *ApJ*, 672, 1054
- Baruteau C., Masset F., 2008b, *ApJ*, 678, 483
- Baruteau C., Meru F., Paardekooper S.-J., 2011, *MNRAS*, 416, 1971
- Bohn A. J., et al., 2020, *ApJ*, 898, L16
- Boley A. C., 2009, *ApJ*, 695, L53
- Boley A. C., Hayfield T., Mayer L., Durisen R. H., 2010, *Icarus*, 207, 509
- Boss A. P., 1997, *Science*, 276, 1836
- Boss A. P., 2013, *ApJ*, 764, 194
- Boss A. P., 2023, *The Astrophysical Journal*, 943, 101
- Cha S.-H., Nayakshin S., 2011, *Monthly Notices of the Royal Astronomical Society*, 415, 3319
- Cloutier R., Lin M.-K., 2013, *MNRAS*, 434, 621
- Delorme P., et al., 2024, *A&A*, 692, A263
- Deng H., Ogilvie G. I., 2022, *The Astrophysical Journal Letters*, 934, L19
- Deng H., Mayer L., Meru F., 2017, *ApJ*, 847, 43
- Deng H., Mayer L., Latter H., 2020, *The Astrophysical Journal*, 891, 154
- Deng H., Mayer L., Helled R., 2021, *Nature Astronomy*, 5, 440
- Durisen R. H., Boss A. P., Mayer L., Nelson A. F., Quinn T., Rice W. K. M., 2007, in Reipurth B., Jewitt D., Keil K., eds, *Protostars and Planets V*. p. 607 ([arXiv:astro-ph/0603179](https://arxiv.org/abs/astro-ph/0603179)), doi:10.48550/arXiv.astro-ph/0603179
- Fletcher M., Nayakshin S., Stamatellos D., Dehnen W., Meru F., Mayer L., Deng H., Rice K., 2019, *Monthly Notices of the Royal Astronomical Society*, 486, 4398
- Forgan D. H., Hall C., Meru F., Rice W. K. M., 2017, *Monthly Notices of the Royal Astronomical Society*, 474, 5036
- Fu Z., Deng H., Lin D. N. C., Mayer L., 2025, *Science Advances*, 11, eadu6058
- Galvagni M., Mayer L., 2013, *Monthly Notices of the Royal Astronomical Society*, 437, 2909
- Galvagni M., Hayfield T., Boley A., Mayer L., Roškar R., Saha P., 2012, *Monthly Notices of the Royal Astronomical Society*, 427, 1725
- Gammie C. F., 2001, *ApJ*, 553, 174
- Goldreich P., Tremaine S., 1979, *ApJ*, 233, 857
- Goldreich P., Tremaine S., 1980, *ApJ*, 241, 425
- Hall C., Forgan D., Rice K., 2017, *Monthly Notices of the Royal Astronomical Society*, 470, 2517
- Hayfield T. J., 2011, PhD thesis, Eidgenössische Technische Hochschule, Zurich, Switzerland
- Helled R., Bodenheimer P., 2011, *Icarus*, 211, 939
- Helled R., Schubert G., 2008, *Icarus*, 198, 156
- Helled R., et al., 2014, Giant Planet Formation, Evolution, and Internal Structure. University of Arizona Press, doi:10.2458/azu_uapress_9780816531240-ch028, http://dx.doi.org/10.2458/azu_uapress_9780816531240-ch028
- Hopkins P. F., 2015, *Monthly Notices of the Royal Astronomical Society*, 450, 53
- Hopkins P. F., 2016, *MNRAS*, 462, 576
- Hopkins P. F., Raives M. J., 2016, *MNRAS*, 455, 51
- Humphries R. J., Nayakshin S., 2018, *Monthly Notices of the Royal Astronomical Society*, 477, 593
- Janson M., et al., 2021, *Nature*, 600, 231
- Johansen A., Lambrechts M., 2017, *Annual Review of Earth and Planetary Sciences*, 45, 359
- Kubli N., Mayer L., Deng H., 2023, *Monthly Notices of the Royal Astronomical Society*, 525, 2731
- Kuiper G. P., 1951, *Proceedings of the National Academy of Sciences*, 37, 1
- Lin D. N. C., Papaloizou J., 1979, *MNRAS*, 186, 799
- Lin D. N. C., Papaloizou J., 1986a, *ApJ*, 309, 846
- Lin D. N. C., Papaloizou J., 1986b, *ApJ*, 309, 846
- Lin M.-K., Papaloizou J. C. B., 2012, *MNRAS*, 421, 780
- Lodato G., Rice W. K. M., 2004, *MNRAS*, 351, 630
- Machida M. N., ichiro Inutsuka S., Matsumoto T., 2011, *The Astrophysical Journal*, 729, 42
- Malik M., Meru F., Mayer L., Meyer M., 2015, *The Astrophysical Journal*, 802, 56
- Marois C., Macintosh B., Barman T., Zuckerman B., Song I., Patience J., Lafrenière D., Doyon R., 2008, *Science*, 322, 1348
- Masset F., 2000, *A&AS*, 141, 165
- Masset F. S., 2008, in Goupil M. J., Zahn J. P., eds, *EAS Publications Series Vol. 29*, *EAS Publications Series*. pp 165–244, doi:10.1051/eas:0829006
- Masset F. S., Papaloizou J. C. B., 2003a, *ApJ*, 588, 494
- Masset F. S., Papaloizou J. C. B., 2003b, *ApJ*, 588, 494
- Matzkevich Y., Reinhardt C., Meier T., Stadel J., Helled R., 2024, *A&A*, 691, A184
- Mayer L., 2013, *Classical and Quantum Gravity*, 30, 244008
- Mayer L., Quinn T., Wadsley J., Stadel J., 2002, *Science*, 298, 1756
- Mayer L., Quinn T., Wadsley J., Stadel J., 2004, *The Astrophysical Journal*, 609, 1045
- Meru F., Bate M. R., 2011, in Sozzetti A., Lattanzi M. G., Boss A. P., eds, *IAU Symposium Vol. 276*, *The Astrophysics of Planetary Systems: Formation, Structure, and Dynamical Evolution*. pp 438–440 ([arXiv:1011.1033](https://arxiv.org/abs/1011.1033)), doi:10.1017/S1743921311020709
- Meru F., Juhász A., Ilee J. D., Clarke C. J., Rosotti G. P., Booth R. A., 2017, *ApJ*, 839, L24
- Michael S., Durisen R. H., Boley A. C., 2011, *ApJ*, 737, L42
- Miret-Roig N., et al., 2022, *Nature Astronomy*, 6, 89
- Müller S., Helled R., Mayer L., 2018, *The Astrophysical Journal*, 854, 112
- Nayakshin S., 2010, *Monthly Notices of the Royal Astronomical Society: Letters*, 408, L36
- Nayakshin S., Fletcher M., 2015, *Monthly Notices of the Royal Astronomical Society*, 452, 1654
- Paardekooper S. J., Papaloizou J. C. B., 2009, *MNRAS*, 394, 2297
- Paardekooper S. J., Baruteau C., Crida A., Kley W., 2010, *MNRAS*, 401, 1950
- Papaloizou J. C. B., Nelson R. P., Kley W., Masset F. S., Artymowicz P., 2007, in Reipurth B., Jewitt D., Keil K., eds, *Protostars and Planets V*. p. 655 ([arXiv:astro-ph/0603196](https://arxiv.org/abs/astro-ph/0603196)), doi:10.48550/arXiv.astro-ph/0603196
- Peplinski A., 2008, PhD thesis, Stockholm University
- Pepliński A., Artymowicz P., Mellema G., 2008, *Monthly Notices of the Royal Astronomical Society*, 387, 1063
- Pérez L. M., et al., 2016, *Science*, 353, 1519
- Pollack J. B., Hubickyj O., Bodenheimer P., Lissauer J. J., Podolak M., Greenzweig Y., 1996, *Icarus*, 124, 62
- Price D. J., Monaghan J. J., 2007, *MNRAS*, 374, 1347
- Riols A., Latter H., 2019, *MNRAS*, 482, 3989
- Rowther S., Meru F., 2020, *Monthly Notices of the Royal Astronomical Society*, 496, 1598
- Safronov V. S., 1972, *Evolution of the protoplanetary cloud and formation of the earth and planets*. Keter Publishing House
- Santos, N. C. et al., 2017, *A&A*, 603, A30
- Schib O., Mordasini C., Helled R., 2023, *A&A*, 669, A31
- Schlecker, M. et al., 2022, *A&A*, 664, A180
- Souza Lima R., Mayer L., Capelo P. R., Bortolas E., Quinn T. R., 2020, *ApJ*, 899, 126
- Speedie J., et al., 2024, *Nature*, 633, 58
- Stamatellos D., 2015, *The Astrophysical Journal Letters*, 810, L11

- Suzuki D., et al., 2018, *ApJ*, 869, L34
 Szulágyi J., Mayer L., Quinn T., 2016, *Monthly Notices of the Royal Astronomical Society*, 464, 3158
 Tanaka H., Takeuchi T., Ward W. R., 2002a, *ApJ*, 565, 1257
 Tanaka H., Takeuchi T., Ward W. R., 2002b, *ApJ*, 565, 1257
 Toomre A., 1964, *ApJ*, pp 1217–1238
 Veronesi B., Paneque-Carreño T., Lodato G., Testi L., Pérez L. M., Bertin G., Hall C., 2021, *ApJ*, 914, L27
 Veronesi B., Longarini C., Lodato G., Laibe G., Hall C., Facchini S., Testi L., 2024, *A&A*, 688, A136
 Vorobyov E. I., Basu S., 2005, *The Astrophysical Journal*, 633, L137
 Wu Y., Chen Y.-X., Lin D. N. C., 2024, *MNRAS*, 528, L127
 Zhu Z., Hartmann L., Nelson R. P., Gammie C. F., 2012, *ApJ*, 746, 110

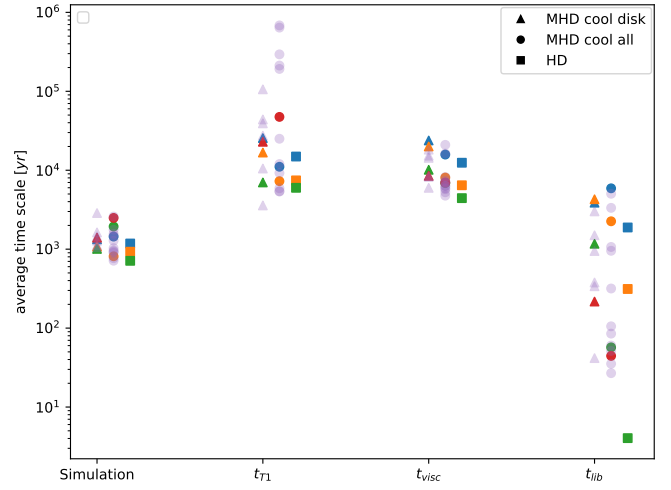


Figure A1. Comparison of different time scales relative to migration time (absolute times of fig. 13).

APPENDIX A: ADDITIONAL FIGURES

This paper has been typeset from a $\text{\TeX}/\text{\LaTeX}$ file prepared by the author.

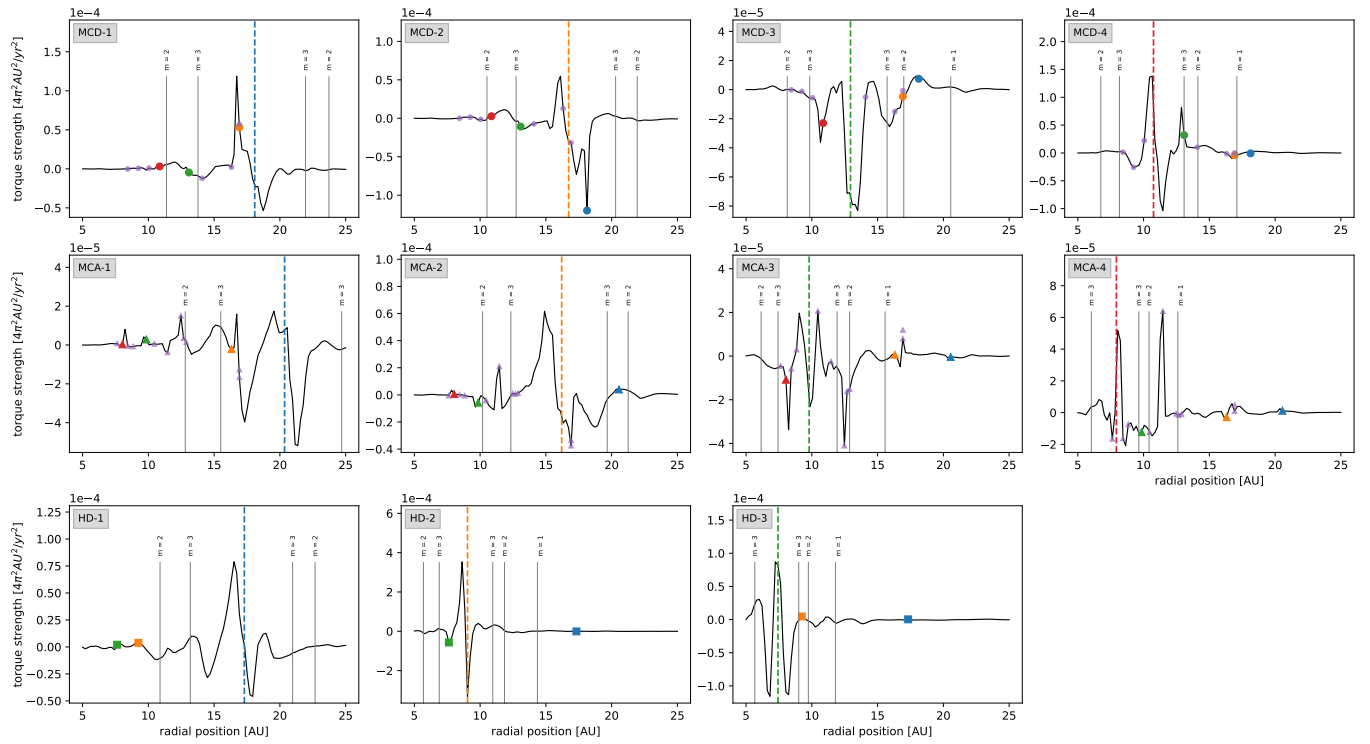


Figure A2. Same as fig. 9 but at $t \sim 199$ yr. The shape of the profile changes fast (e.g. the spike to the interior of MCA-1 that exists in fig. 9 has disappeared after half an orbit).